Naturally forced multidecadal variability of the Atlantic meridional overturning circulation

Matthew B. Menary · Adam A. Scaife

Abstract The mechanisms by which natural forcing factors alone could drive simulated multidecadal variability in the Atlantic meridional overturning circulation (AMOC) are assessed in an ensemble of climate model simulations. It is shown for a new state-of-the-art general circulation model, HadGEM2-ES, that the most important of these natural forcings, in terms of the multidecadal response of the AMOC, is solar rather than volcanic forcing. AMOC strengthening occurs through a densification of the North Atlantic, driven by anomalous surface freshwater fluxes due to increased evaporation. These are related to persistent North Atlantic atmospheric circulation anomalies, driven by forced changes in the stratosphere, associated with anomalously weak solar irradiance during the late nineteenth and early twentieth centuries. Within a period of approximately 100 years the 11-year smoothed ensemble mean AMOC strengthens by 1.5 Sv and subsequently weakens by 1.9 Sv, representing respectively approximately 3 and 4 standard deviations of the 11-year smoothed control simulation. The solar-induced variability of the AMOC has various relevant climate impacts, such as a northward shift of the intertropical convergence zone, anomalous Amazonian rainfall, and a sustained increase in European temperatures. While this model has only a partial representation of the atmospheric response to solar variability, these results demonstrate the potential for solar variability to have a multidecadal impact on North Atlantic climate.

M. B. Menary (✉) · A. A. Scaife
Met Office Hadley Centre, Met Office, Fitzroy Road,
Exeter, Devon EX1 3PB, UK
e-mail: matthew.menary@metoffice.gov.uk

1 Introduction

The large-scale ocean circulation in the North Atlantic Ocean is partly responsible for the relative warmth of the western Eurasian continent as opposed to similar latitudes in North America (Knight et al. 2005; Sutton and Hodson 2005; Pohlmann et al. 2006). This circulation is simplified by reducing the 3-dimensional ocean circulation into a 2-dimensional overturning streamfunction in the depth-latitudinal plane, denoted the Atlantic meridional overturning circulation (AMOC) (Kuhlbrodt et al. 2007). To help characterize temporal changes this is often further simplified to the maximum of this circulation at a particular latitude, typically chosen to be 30°N. Changes in the strength of the AMOC have been linked to shifts in the inter-tropical convergence zone (ITCZ) (Vellinga and Wu 2004), large temperature changes over the northern hemisphere (Mignot et al. 2007; Vellinga and Wood 2008; Wood et al. 2003), changes in El-Niño (Timmermann et al. 2007; Dong et al. 2006), sea level rise (Levermann et al. 2005), drought in the Sahel region and changes in Atlantic hurricane activity (Zhang and Delworth 2006). Models suggest the AMOC has variability on all timescales, forced by Ekman pumping (Jayne and Marotzke 2001), changes in deep water convection strength (Dong and Sutton 2005), and slow advective timescales from the subtropics (Menary et al. 2012). Evidence from the paleo record suggests dramatic weakenings are possible (Moreno et al. 2010; McManus et al. 2004) with models and observational analyses also suggesting the AMOC may exhibit bistability (Hawkins et al. 2011). Despite this, statistically significant changes in the strength of the AMOC may not be detectable for many decades (Roberts and Palmer 2012). Thus, given the large impacts and variability, understanding the past behaviour of the AMOC is crucial in understanding

potential future climate change (Rahmstorf 2003). Anthropogenic emissions of greenhouse gases and aerosols since industrialization are very likely responsible both for much of the upward trend in observed global average temperature (Meehl et al. 2007) and, more recently, some aspects of Atlantic multidecadal variability (Booth et al. 2012). However, multidecadal variability in the AMOC could modulate some temperature changes on a hemispheric and perhaps global scale (Zhang and Vallis 2007; Semenov et al. 2010). Recently it has been shown that elements of AMOC variability may even be driven from the stratosphere (Manzini et al. 2012; Reichler et al. 2012). Increased mechanistic understanding of forced AMOC changes are therefore important to better understand past climate events and to anticipate future events.

Previous modelling studies have suggested that solar forcing may weaken (Swingedouw et al. 2011; Goosse and Renssen 2006), strengthen (Sedlacek and Mysak 2009), or have little effect on the AMOC (Zorita et al. 2004), at various timescales. The AMOC response to volcanic forcing is equally poorly constrained, with some models suggesting the response to volcanic forcing is a weakening (Zhong et al. 2011), some a strengthening (Stenchikov et al. 2009; Iwi et al. 2012), while others that the response is a function of the period and strength of the volcanic forcing (Mignot et al. 2011) or the background state (Zanchettin et al. 2011). The current study focuses on the climate response to naturally forced changes in climate and the AMOC since the mid 19th Century. Although the model includes, for example, the latest representations and treatment of tropospheric chemistry and aerosols appropriate for the CMIP5 ensemble one of the limitations is a relatively poorly resolved stratosphere. Nonetheless, through a mechanistic understanding of the interaction between natural (solar and volcanic) forcings and the AMOC, this study demonstrates the potential for solar variability to affect regional climate on multidecadal timescales.

The paper is structured as follows: Sect. 2 describes the model and experimental design and Sect. 3 briefly describes the response of the AMOC. Section 4 details the important oceanic and atmospheric mechanisms as well as additional sensitivity experiments. Large scale climatic responses are discussed in Sect. 5 before conclusions in Sect.6.

## 2 Model description and experimental setup

This paper uses results from the latest fully coupled atmosphere-ocean general circulation model (AOGCM) from the UK Met Office Hadley Centre: HadGEM2-ES [Hadley Centre Global Environmental Model 2, with

Earth-System components (Collins et al. 2011; Jones et al. 2011)]. This model represents a considerable improvement on previous versions of the model [e.g. HadCM3 (Gordon et al. 2000), HadGEM1 (Johns et al. 2006)] in that it includes interactive chemistry in the troposphere through the United Kingdom Chemistry and Aerosols (UKCA) sub-model (Morgenstern et al. 2009), improved representation of the direct and indirect effects of aerosols (Bellouin et al. 2011), and an improved ocean-atmosphere-land carbon cycle (Jones et al. 2011). Additionally, the model includes improvements to the physical model to improve the representation of El-Niño and northern hemisphere land surface temperatures (Martin et al. 2011). The model resolution in the atmosphere is $1.875° \times 1.25°$ with 38 vertical levels and the model lid at 40km. This limits the representation of the upper stratosphere where solar heating is largest. In the ocean the model has a resolution of $1° \times 1°$, increasing near the equator to $1/3°$ in latitude, with 40 vertical levels.

Along with a 1,041 year pre-industrial control simulation, this study uses two parallel sets of simulations including various combinations of external forcings. Each is a 4-member ensemble of 150 years beginning in the year 1859, initialised at 50 year intervals from within the model pre-industrial control simulation. Unless otherwise stated, all results are quoted as the ensemble mean of the particular 4-member ensemble with annual means used for oceanic indices and wintertime (December, January, February) seasonal means used for atmospheric indices. The forcing sets are as follows: NAT, which includes the natural forcings of solar variability and volcanic emissions; NOSOL, in which the solar variability is removed. For each member of the NAT ensemble there is a member of the NOSOL ensemble with identical initial conditions. Extra NAT simulations were performed for the period 1859–1920 to test whether the AMOC strengthening was sensitive to the choice of stratospheric ozone specification and are described in Sect. 3. Additionally, sensitivity experiments were conducted which used an interannually constant solar forcing at various levels to further help determine the atmospheric response to solar forcing. These are described further in Sect. 4.3.

The 11-year solar cycle is applied to all of the NAT ensemble members through the amount of incident solar energy at the top of the atmosphere (the Total Solar Irradiance, TSI). Additionally, in two of the ensemble members only, the solar cycle is manifest indirectly through the specification of stratospheric ozone. The TSI is spread across six spectral bands, varying in wavelength from 200 nm to 10 μm as described in Jones et al. (2011) and Stott et al. (2006). Tropospheric ozone is controlled interactively through UKCA. In NAT ensemble members 3 and 4 the stratospheric ozone is specified using the ALL-

Fig. 1 **a** Normalised monthly
mean volcanic aerosol optical
depth forcing, applied through 4
equal area bands, and **b** time
series of annual mean total solar
irradiance (TSI) in (*blue*) NAT
and (*orange*) NOSOL
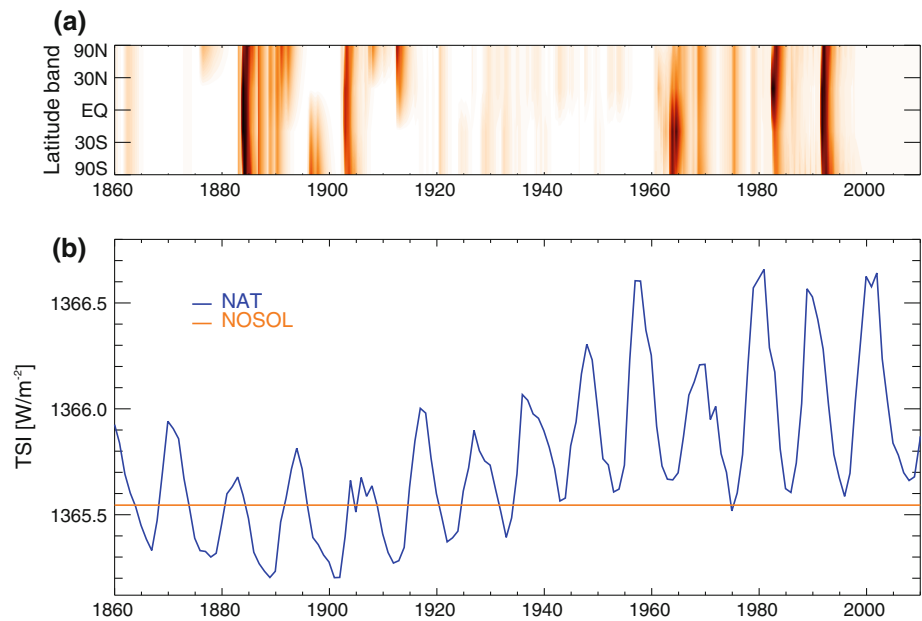
**Table 1** Summary of simulations performed during this analysis

	Length or period (years)	Ensemble size	11-year solar cycle	
Control	1,041	1	No	No interannually varying solar or volcanic forcing
NAT	1859–2010 (Initialised at 50 years intervals)	4	Yes	Solar cycle additionally input through specification of time varying stratospheric ozone in two of these simulations
NOSOL	1859–2010 (initialised at 50 years intervals)	4	No	Volcanic forcing only
First sensitivity test: specification of stratospheric ozone	1859–1920 (initialised at 50 year intervals)	6	Yes	Solar cycle additionally input through specification of time varying stratospheric ozone
Second sensitivity test: magnitude of constant solar forcing	20 (Identical initial conditions)	7	No	See Sect. 4.3

forcings experiment (Jones et al. 2011). In the ALL-forcings experiment the stratospheric ozone was estimated by regressing chlorine concentrations and a solar index against available observations and these scaling factors used to estimate stratospheric ozone at any time (Jones et al. 2011). Subsequently just the solar index scaling factor was used to construct the stratospheric ozone for NAT ensemble members 3 and 4. Stratospheric ozone in NOSOL and in NAT ensemble members 1 and 2 is specified as a seasonally varying climatology from the control simulation which does not include any interannual variability. Volcanic emissions are after Sato et al. (1993) and as also described in Jones et al. (2011). Time series of TSI and normalised volcanic aerosol optical depth are shown in Fig. 1. Note the Krakatoa volcano in 1883 and the subsequent period of very little volcanism in the first half of

the 20th Century. In NAT the low frequency TSI decreases over the first 50 years and then increases until 1980. The amplitude of the 11-year solar cycle follows a similar evolution. For clarity TSI is plotted as an annual mean but the climatological seasonal range is from 1,322 to 1,410 Wm^{-2}. Table 1 summarises the simulations analysed.

3 AMOC response

The AMOC in the pre-industrial control simulation of HadGEM2-ES has a mean of 13.8 Sv and a standard deviation (of annual mean data) of 1.0 Sv over a period of 1,041 years [13.6 Sv with a standard deviation of 1.0 Sv for the first 500 years (Menary et al. 2013)]. Drifts are essentially zero at (0.061 ± 0.028) Sv/Century. Measured
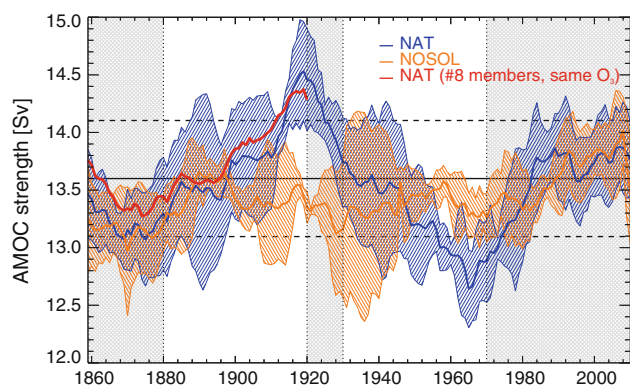
Fig. 2 Time series of 11-year running mean AMOC strength at 30°N in (*blue*) NAT and (*orange*) NOSOL. *Line shading* represents one standard deviation of the 4-member model ensemble. Areas without *grey shading* highlight the two time periods (1880–1920 and 1930–1970) separately analysed in the text. Also plotted are (*black, solid*) the mean AMOC strength in the control simulation, (*black, dashed*) the 11-year running mean one standard deviation range, and (*red*) the ensemble mean of the 8-member (6 sensitivity simulations + 2 identically forced simulations from the original NAT ensemble) ensemble from 1859–1920 with all members using the same specification of stratospheric ozone

since 2004, direct observations using the RAPID array (Cunningham et al. 2007) put the AMOC strength at (18.7 ± 2.1) Sv (Kanzow et al. 2010), higher than in the control simulation. However, the model control AMOC is representative of a pre-industrial rather than present-day climate. Recent work using the ALL forcings ensemble with HadGEM2-ES has shown that the modelled AMOC response to anthropogenic forcings over the last 150 years has been to strengthen, reaching a value of around 16 Sv towards the end of the 20th Century, more in line with the recent direct observations (Menary et al. 2013). This highlights the potential pitfalls in comparing pre-industrial and present-day strengths of the AMOC and, in this particular case, the multidecadal sensitivity of the AMOC in HadGEM2-ES to past external forcings.

The response of the AMOC to the natural climate forcings is to increase from around 13 Sv in the first decade of the simulation to a maximum 11-year mean of 14.5 Sv in the early 20th Century over a period of around 50 years (Fig. 2, blue). Here and throughout, 11-year means are used for the AMOC to remove some of the interannual, sub-decadal variability that is not the focus of this study. Subsequently, over a similar length of time, the AMOC decreases to a minimum 11-year mean value of 12.6 Sv in the 1960s. In contrast, the response of the AMOC to volcanic forcing only is markedly reduced, with no clear signal of a long term rise or decline (Fig. 2, orange). The standard deviation of the 11-year mean control simulation is 0.5 Sv and the AMOC in NAT exhibits sustained periods outside of this range. A further test of the significance of

this AMOC strengthening and decline is made by conducting a bootstrapping Monte-Carlo test using the 500 years of the control simulation parallel to these experiments. Here, 10,000 pseudo-ensembles (each of 4 members) are created from the control simulation with randomly selected start points to mimic the ensemble design. The distribution of 50-year long AMOC trends is then calculated from these 10,000 control pseudo-ensembles. This suggests a 0.3 % chance of producing an AMOC strengthening of this magnitude in NAT simply through internal variability.

In addition to the NAT and NOSOL ensembles, a further set of six simulations using the NAT forcings were conducted up to 1920 using the time varying stratospheric ozone already applied in ensemble members 3 and 4 to test the effect of using constant or time-varying stratospheric ozone. These combine to give an eight member ensemble of identically forced simulations with the only difference the initial conditions taken at 50-year intervals from the control simulation. The ensemble mean AMOC strength of this set of experiments also rises in a similar fashion to the original ensemble (Fig. 2, red) suggesting the choice of stratospheric ozone specification is not a crucial factor. Thus we continue to analyse the original 4-member NAT ensemble in the remaining text as this is parallel to the NOSOL ensemble which allows for direct comparisons between the two sets of experiments.

4 Mechanisms

We now investigate the mechanisms behind this AMOC response to natural climate forcings. Section 4.1 explores the oceanic changes leading the AMOC strengthening and subsequent weakening in NAT and Sect. 4.2 details the associated surface atmospheric changes. Subsequently, the link between lower and upper atmosphere is investigated with help from sensitivity experiments in Sect. 4.3. A summary of the mechanism is given in Sect. 4.4 with a note on the AMOC weakening phase in Sect. 4.5.

4.1 Oceanic component

The AMOC strengthening/weakening in NAT is associated with a reduction/increase of stratification in the Labrador Sea, which has been shown to be a precursor to strengthening of the AMOC in a range of CMIP5 model control simulations (Roberts et al. 2013) and leads the AMOC by around one decade. This deep convection appears as a series of large events with a gradual upwards trend in the late 19th and early 20th centuries and a subsequent gradual downwards trend towards the middle of the 20th century, though particular years may have more or less Labrador
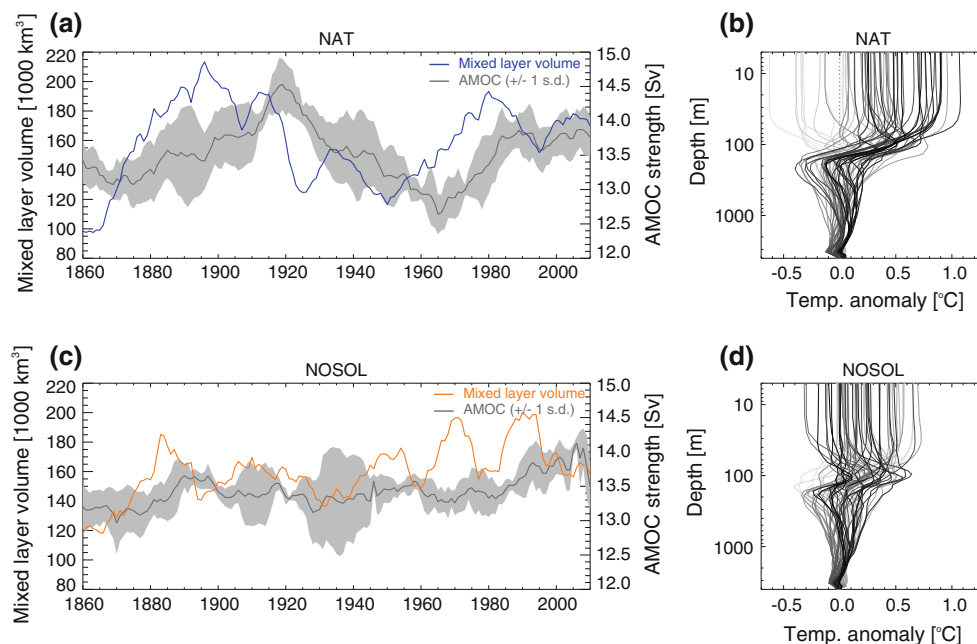
Fig. 3 Extended Labrador Sea region (60°W–45°W, 50°N–65°N) mixed layer volume (area-total of mixed layer depth) in **a** NAT and **c** NOSOL for the month of March, *left axis*. On *right axis* is 11-year running mean AMOC strength at 30°N with *shading* representing intra-ensemble standard deviation, as in Fig. 2. Mixed layer calculated after Kara et al. (2000) using a cutoff value of 0.2 °C. **b** NAT and **d** NOSOL ensemble mean March-time Labrador Sea temperature anomalies for the first 60 years of the experiments with later periods drawn increasingly *dark*

Sea convection. These changes in convection are seen in the NAT ensemble (Fig. 3a) but not in NOSOL (Fig. 3c) although there is some century timescale drift in the NO-SOL ensemble. Due to the increased deep convection in the model sinking regions, the AMOC strengthens, from an initial value of 13 Sv to a maximum ensemble mean 11-year average of 14.5 Sv. Similarly, associated with the AMOC weakening in NAT of 1.9 Sv between 1930 and 1970 is a prior reduction in convection; the reasons for this are now discussed.

The increase in deep convection in NAT up to the beginning of the 20th century is driven by an increase in the near surface density of the Labrador Sea (Fig. 4a) which acts to destabilize the water column. Consistent with the deep convection figure, there is little change in the density of the near surface Labrador Sea in NOSOL (Fig. 4b) during this time. An increase in density in NAT could be due to an increase in salinity or a decrease in temperature of this part of the water column. To determine the cause, the density time series in Fig. 4 are further decomposed into components driven by salinity and temperature. This is achieved by respectively time averaging temperature and salinity in the equation of state, whilst letting the other vary, after Delworth et al. (1993). Although the equation of state is non-linear, small perturbations at these values of temperature and salinity yield a good approximation with a correlation between the actual integrated density anomalies and the sum of the anomalies in the two linearised cases greater than $r = 0.99$. Thus it can be seen from Fig. 4 that salinity (dotted) is the important driver of the modelled density change in this region prior to the AMOC maximum around 1920. In this context the warming of the near surface ocean actually acts to oppose this salinity increase, but the salinity effects dominate. After 1920 the AMOC in NAT weakens which is preceded by a decline in the near surface density. This is related to a combination of surface salinity fluxes and the gradual increase of advective heat fluxes and is discussed in Sect. 4.5. Note also that the gradual salinification (densification) in the period 1880–1920 merely acts to modify the background state so that particular convective events can become increasingly frequent and that individual convective events in particular winters are likely related to anomalous heat rather than salinity fluxes.

The near surface salinification in NAT is associated with an increase in evaporation. Anomalous net precipitation minus evaporation (P–E) fluxes over the Labrador Sea are greater than the anomalous fluxes of freshwater from ice melt and runoff (not shown) resulting in a net decrease in surface freshwater fluxes and thus an increase in surface salinity (Fig. 5). The evaporation increase is much larger in NAT (Fig. 5a) than in NOSOL (Fig. 5b), and in NAT is only partially offset by an increase in precipitation (over more coastal regions) so that there is a fall in the net P–E.
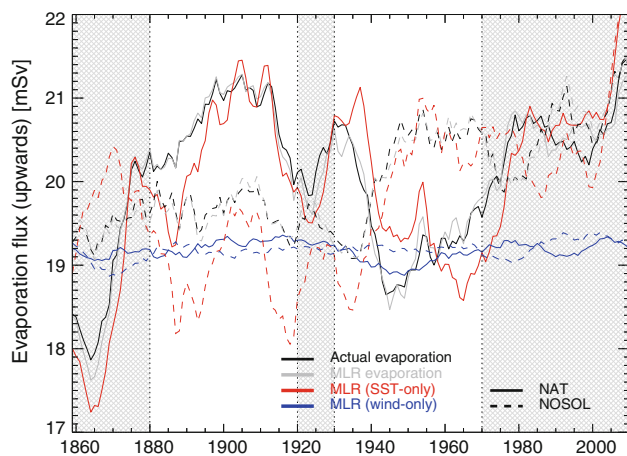
Fig. 4 Extended Labrador Sea region (60°W–45°W, 50°N–65°N) 11-year running mean top 800 m-average density anomaly (relative to first 2 decades) in (**a**) NAT and (**b**) NOSOL. On *left axis* is density computed in three ways: (*solid*) normal, (*dot-dashed*) using time-averaged salinity to show temperature effects, and (*dotted*) using time-averaged temperature to show salinity effects. Additionally, the linear sum of the time-averaged salinity and time-averaged temperature anomalies is overplotted in *dashed black* for NAT. On *right axis* is 11-year running mean AMOC strength at 30°N with *shading* representing intra-ensemble standard deviation, as in Fig. 2
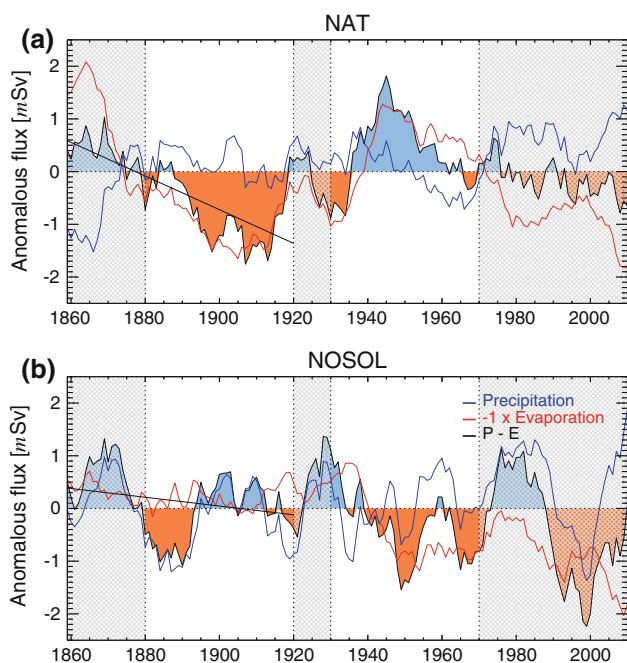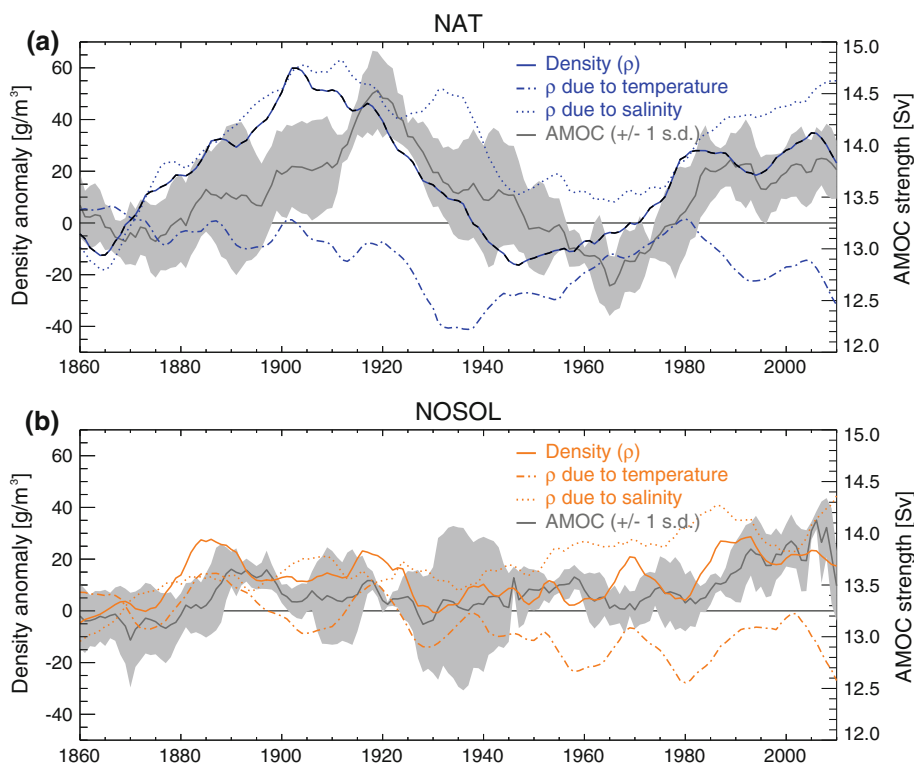
Fig. 5 11-year running mean time series of anomalous precipitation (P), evaporation (E), and net P–E relative to the first 30 years into the Labrador Sea region (60°W–45°W, 50°N–65°N) in (**a**) NAT and (**b**) NOSOL. Also plotted are trends for the first 60 years (*black, solid*). Anomalously negative P–E periods (associated with salinification) are *shaded orange* and anomalously positive P–E periods (associated with freshening) are *shaded blue*. Areas without *grey shading* highlight the two time periods (1880–1920 and 1930–1970) separately analysed in the text

The trend in net P–E into the Labrador Sea from the beginning of the simulations to 1920 is approximately 4 times larger in NAT than in NOSOL. There is possibly also a component of the increased salinity and temperature related to the positive feedback of a strengthening AMOC bringing more salty and warm water northwards. Analysis of Fig. 4 suggests though that this is limited prior to 1920 otherwise temperature effects on density would be playing a more negative role. The periods of AMOC strengthening in NAT (1880–1920) and weakening (1930–1970) are highlighted by the removal of grey shading and are analysed in more detail in the following sections. In this figure these two periods correspond to anomalous decreases and increases in net P–E into the Labrador Sea respectively.

To elucidate the driver behind the evaporation changes in NAT, multiple linear regression (MLR) of area-averaged components of the evaporation equation over the Labrador Sea was performed. This was done using the 1,041 years of the control simulation and comprised the following four input variables, plus a constant: SSTs, surface humidity, surface wind speed, and ice cover. Despite the simplification of using MLR rather than the actual evaporation equation (which would not have been exact regardless as only monthly mean diagnostics were stored from the simulations) the diagnosed evaporation and the MLR-derived evaporation agree very well (black and grey lines respectively in Fig. 6). Having computed the regression coefficients for the four variables it was then possible to hold

Fig. 6 11-year running mean time series of various evaporation metrics directed out of the Labrador Sea region (60°W–45°W, 50°N–65°N) in (*solid*) NAT and (*dashed*) NOSOL. The metrics are: (*black*) actual model diagnosed evaporation; (*grey*) evaporation calculated using area-averaged SST, 10 m wind, ice cover, and humidity combined using multiple linear regression (MLR) with coefficients ascertained from the control simulation; (*red*) as the former but only allowing SSTs to vary with time and holding 10 m wind, ice cover, and humidity at constant values; (*blue*) as the former but now instead only allowing wind to vary with time and holding SST, ice cover, and humidity at constant values. Areas without *grey shading* highlight the two time periods (1880–1920 and 1930–1970) separately analysed in the text

various combinations of the components constant to estimate their relative importance with the cases of time-varying SSTs-only and time-varying surface winds-only plotted on Fig. 6. The actual model evaporation time series (black line) can be reconstructed well using only time-varying SSTs, suggesting the increase in evaporation in NAT is mainly related to SST changes, with the direct effect of wind changes playing a minor supporting role (although we will show shortly that they play an important indirect role). The two periods of interest are again highlighted with the removal of grey shading and show that SST-driven evaporation increases in the first period (1880–1920) and decreases in the second period (1930–1970), with this change particularly pronounced when considering the difference between NAT (solid lines) and NOSOL (dashed lines). For the second period there are complicating effects due to a potential AMOC feedback bringing more warm water northwards which may be the cause of the slight disparity between MLR (SST-only, red) and MLR (full, grey) during this time.

It therefore appears that SSTs in NAT are driving the changes in Labrador Sea evaporation. The actual SSTs in the Labrador Sea show a high correlation with the SST-induced evaporation changes for both NAT and NOSOL, with correlations of $r = 0.94$ and $r = 0.99$ respectively. Also associated with the warming is a reduction in winter sea ice in the Labrador Sea (not shown) which both acts to

directly freshen the surface waters and to expose more of the ocean to evaporation and heat loss. Possible atmospheric drivers of this increase in SSTs in NAT are now investigated.

4.2 Atmospheric component

Although available diagnostics preclude the completion of a full, closed heat budget, the temperature profiles in the Labrador Sea strongly suggest that the source of the surface warming is increased mixing of warmer water from depth. Figure 3b, d shows the anomalous temperature profiles in the Labrador Sea for the month of March, from the beginning of the simulations up to 1920, with later dates drawn increasingly dark. In NOSOL there is little structure to the anomalies, except perhaps an indication of some slow migration of the depth of the thermocline, indicated by relative warming at 100 m and cooling at 150 m. However, in NAT there is a clear signal of near surface warming which generally increases through time and is counterbalanced by cooling at depths greater than 100m, indicative of increased mixing. This is because in the mean state there is a subsurface thermal maximum in the Labrador Sea in wintertime and so an increase in mixing is associated with surface warming and subsurface cooling. We now discuss surface wind anomalies as the potential driver of this increased mixing.

Wind speed changes can have competing effects on SSTs, depending on their strength and the mean temperature profile of the underlying ocean. Ignoring mixing, increases in surface winds would cool the surface ocean via latent heat loss. However, in the presence of a subsurface thermal maximum in the ocean, such as that in the Labrador Sea, stronger surface winds could warm the surface ocean by promoting increased mixing of the cool surface and warmer subsurface waters. As shown in Fig. 6, the first, latent-heat method of wind forcing of the ocean does not appear to be of primary importance in terms of driving the SST/evaporation changes seen in the NAT simulations. Inspection of Fig. 3, particularly panel b, suggests though that the second mechanism may be crucial here in causing the increase in Labrador Sea SSTs as warm water is mixed up from depth. Additionally, Fig. 6 shows that although the direct contribution of wind-forcing to the evaporation is minimal, the winds and evaporation are still positively correlated (see for example the dip in NAT 1930–1970), hinting at coupling via some other mechanism—namely increased wind mixing.

To investigate the role of wind forcing, time means of wintertime 10 m wind speed anomalies are shown in Fig. 7 for NAT and NOSOL in the two periods of interest previously defined. Consistent with the discussion above, there is an increase in surface wind speed magnitudes over the

Fig. 7 Anomalous (relative to full simulation wintertime mean) wintertime 10 m wind magnitude (*shading*) and direction (*vectors*; only vectors greater in magnitude than 0.15 m/s are plotted for clarity) in **a**, **c** NAT and **b**, **d** NOSOL for the periods **a**, **b** 1880–1920 and **c**, **d** 1930–1970
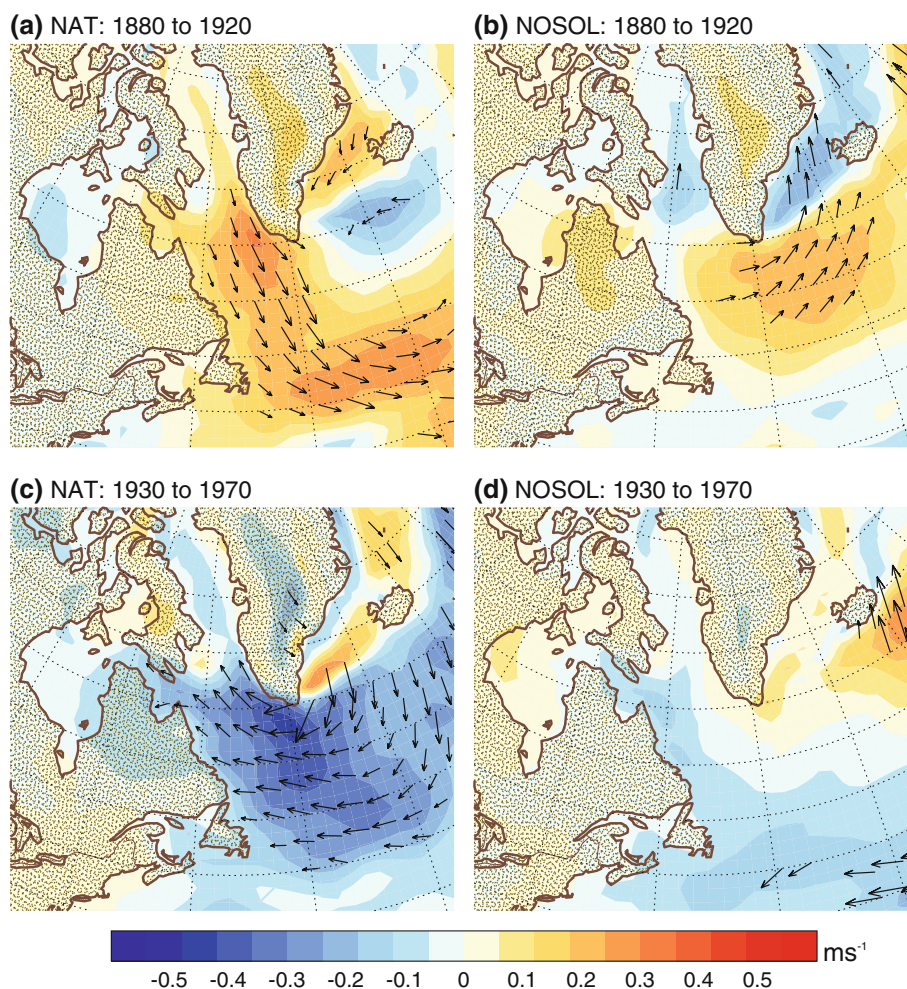
Labrador Sea in NAT for the 40-year period of AMOC strengthening (Fig. 7a), as well as a similar decrease during the 40-year period of AMOC weakening (Fig. 7c). These signals are not seen in NOSOL (Fig. 7b, d) although there is a smaller westerly anomaly over the subpolar gyre in NOSOL for the period 1880–1920. Thus the wind anomalies are consistent with wind-induced mixing being the cause of the SST anomalies, which themselves drive the evaporation and salinification of the Labrador Sea.

The modelled wind speed anomalies are also associated with anomalies in mean sea level pressure (MSLP). For comparison with Fig. 7, plots of time mean wintertime MSLP anomalies are shown in Fig. 8. Statistical significance is estimated from the control simulation by creating 100,000 pseudo-ensembles from the 500 years of control data parallel to these simulations and subsequently marking wherever the data in Fig. 8 falls in the top or bottom 5 % of the control distribution (i.e. significance at the 10 % level). These MSLP patterns are consistent with the wind anomalies for both NAT and NOSOL, but highlight that the two periods are not directly symmetrical and also suggests that

neither period projects directly on to the Icelandic centre of the NAO pattern (NAO: MSLP difference between the Azores and Iceland) in NAT (Fig. 8a, c). Additionally, the Azores high part of the NAO pattern reveals no clear signal (not shown). It is also interesting to note that the signal in NOSOL appears similar to that in NAT, albeit at a far reduced magnitude and with the packed isobars over the Labrador Sea crucially lacking. The origins of these surface pressure/wind anomalies are now investigated with sensitivity experiments.

4.3 Origin of surface atmospheric anomalies

A set of 20-year long sensitivity experiments were conducted to test the atmospheric response to various levels of sustained solar forcing but without the 11-year solar cycle. These are detailed in Table 2. The setup of these experiments was the same as the first NAT ensemble member but without volcanic forcing and with the inclusion of extra model diagnostics and a constant offset in solar irradiance up to ± 1.5 W/m^2. The 11-year solar cycle is not present

Fig. 8 Anomalous (relative to full simulation wintertime mean) wintertime mean sea level pressure (MSLP) in **a**, **c** NAT and **b**, **d** NOSOL for the periods **a**, **b** 1880–1920 and **c**, **d** 1930–1970. Hatching depicts data significant at the 10 % level as described in the text
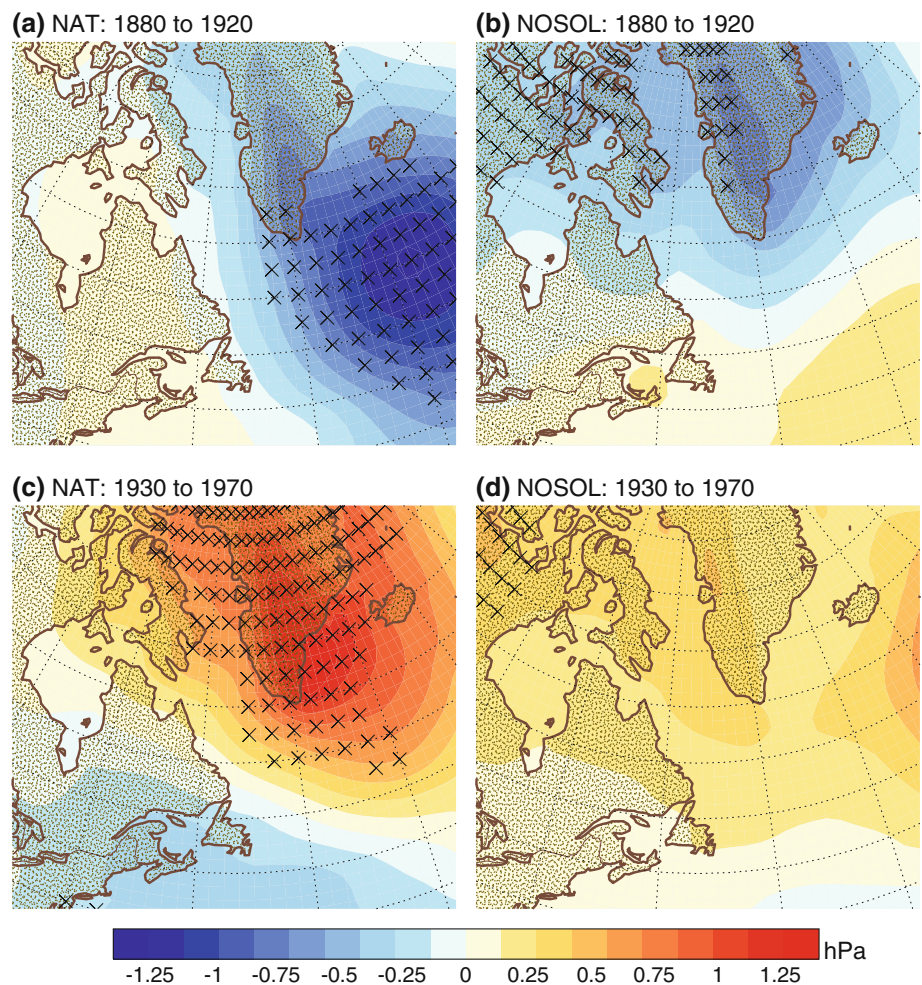
**Table 2** Total solar irradiance in the seven 20-year sensitivity experiments

Sensitivity run	Annual mean total solar irradiance (W/m^2)
SOLAR 0	1,365.5
SOLAR +1	1,366.0
SOLAR +2	1,366.5
SOLAR +3	1,367.0
SOLAR −1	1,365.0
SOLAR −2	1,364.5
SOLAR −3	1,364.0

in these simulations. Stratospheric ozone is applied as an interannually constant climatology as in the first two NAT ensemble members. In order to remove effects due to varying initial conditions these experiments were all initialised from the same point in the control simulation. In the subsequent analysis the difference is taken between the average of the two lowest solar forcing ensemble members (SOLAR −2 and SOLAR −3) and the average of the two highest solar forcing ensemble members (SOLAR +2 and

SOLAR +3) over the 20-year period to estimate the climate model's response to interannually constant solar forcing.

Climatologically, during the northern hemisphere wintertime, the simulated zonal wind is characterised by a tropospheric jet centred around 30°N and 200 hPA and a stratospheric jet centred around 60°N and increasing to 10 hPA. The model lid (top of atmosphere) is at 10 hPa, in-keeping with all the HadGEM2-ES CMIP5 historical ensembles, and represents the bare minimum in stratospheric resolution. There is an order of magnitude greater interannual variability in the winter stratospheric jet than tropospheric jet.

Composites of the difference between the low and high solar forcing cases are shown in Fig. 9 for northern hemisphere wintertime. These experiments show that, in this model and over a long term time mean (i.e. this is not a transient response and not explicitly related to the periodic nature of the 11-year solar cycle), low or reduced solar forcing is consistent with reduced polar temperatures and thus an increase in the meridional temperature gradient (Fig. 9a). This increased temperature gradient is thus

Sensitivity experiments: LOW-SOLAR minus HIGH-SOLAR
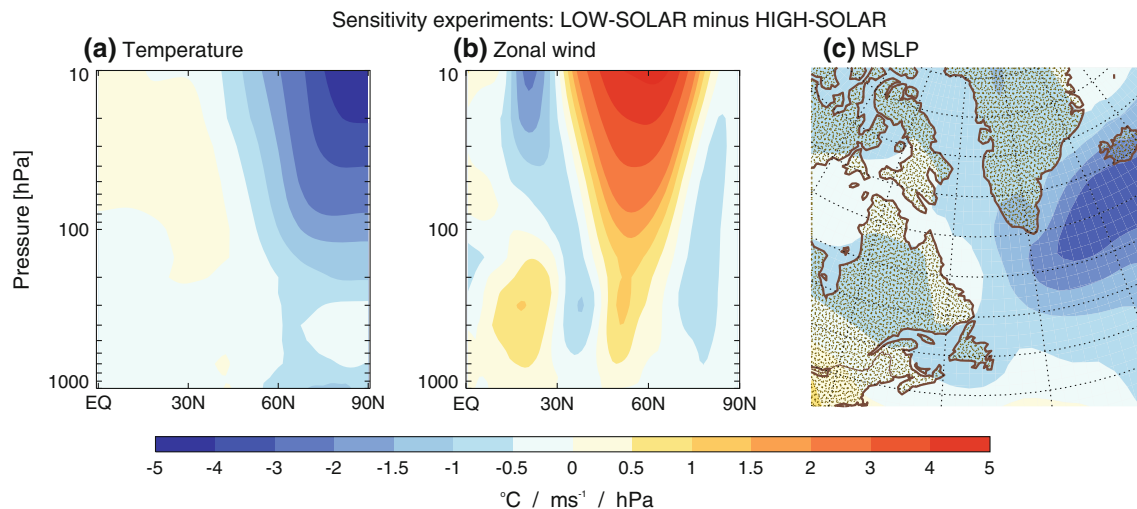
Fig. 9 Composite differences between 20-year time mean (wintertime only) low solar forcing sensitivity experiments (average of SOLAR −2 and SOLAR −3) and high solar forcing sensitivity experiments (average of SOLAR +2 and SOLAR +3). **a** Zonal mean temperature difference, **b** zonal mean zonal wind difference, **c** mean sea level pressure (MSLP) difference

related to westerly wind anomalies in the upper atmosphere which appear to penetrate into the lower troposphere (Fig. 9b) with westerly wind anomalies in the mid to high latitudes and the associated anomaly in MSLP over Greenland and Iceland (Fig. 9c). These responses to solar forcing are consistent in sign and pattern with those in NAT although the signals in NAT are much weaker (not shown) which may be due to the additional presence of the 11-year solar cycle, volcanic forcing, or the internal variability associated with differing start dates in the NAT ensemble. Thus we note that the stratospheric part of the reported mechanism remains tentative.

That the temperature anomaly (at the pole) and the maximum absolute change in wintertime shortwave heating rate (at the equator) are not colocated suggests an important role for the dynamics in setting the polar temperature anomaly and increasing the meridional temperature gradient. Computation of the northern hemisphere Brewer Dobson circulation (BDC) in the sensitivity experiments shows that low solar forcing results in a weakening of the BDC by 0.2×10^9 kg/s compared to high solar forcing. The positive relationship between BDC strength and solar forcing magnitude in these model simulations conflicts with the standard view of weaker BDC during stronger solar forcing (Kodera and Kuroda 2002). Subsequently, regression analysis with the control simulation (not shown) confirms that in the model a reduction in the BDC of this magnitude is consistent with both the patterns and magnitudes of the temperature and zonal wind anomalies seen in the sensitivity experiments in Fig. 9. Diagnostics to compute the BDC were not stored in the original NAT ensemble.

Additionally, another factor involved in the change in polar temperatures is the frequency of wind reversals in the

polar stratosphere. These wind reversals are associated with a break down of the polar vortex, allowing warming of the polar stratosphere, and often called stratospheric sudden warmings (SSWs: defined as reversals in the zonal wind at 10 hPa and 60°N). In the NAT ensemble there are fewer of these than in the NOSOL ensemble prior to 1940 (consistent with polar cooling in NAT) and subsequently more of them after 1940 (consistent with polar warming in NAT).

Thus, although the shortwave heating anomalies are located at the equator, a concomitant change in northward heat transport in this model results in little equatorial temperature change whilst inducing anomalous temperatures in the polar upper atmosphere. Prior to 1920 the annual mean TSI is generally reduced in NAT compared to the climatology in NOSOL which, associated with a reduction in the upper atmosphere poleward heat transport and a change in frequency of SSW events, is related to the polar cooling. Post 1920 the TSI in NAT is generally increased compared to NOSOL and appears to have a consistent and opposite effect in terms of the downstream effect on the AMOC. These signatures are different to what has been found in high top models [and are in some cases of opposite sign, e.g. Ineson et al. (2011)] so while this is a longer timescale, and while the results show the potential for the impact of solar variability on the AMOC, their structure must therefore be taken with caution.

4.4 Summary of mechanism

A schematic of the mechanism is illustrated in Figure 10 for the case of anomalously low solar forcing. In summary, the proposed mechanism is as follows (noting that the
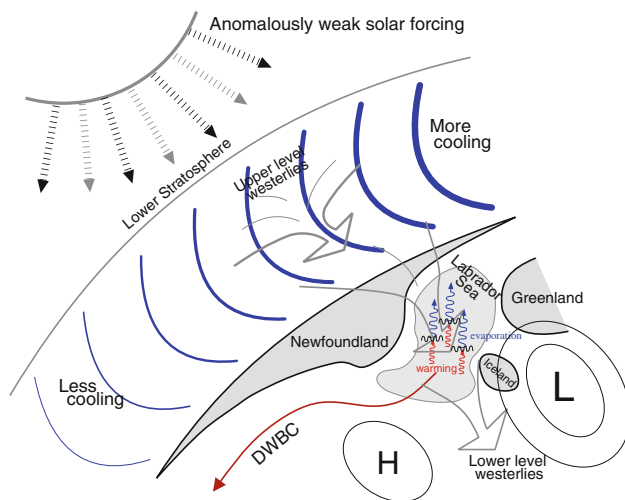
Fig. 10 Schematic illustrating the mechanism for solar-induced multidecadal modulation of the AMOC as it exists in the NAT simulations with the HadGEM2-ES climate model as described in Sect. 4.4

stratospheric part of the mechanism remains tentative): a change in solar forcing leads to a change in the upper atmosphere northern hemisphere wintertime meridional temperature gradient. This is associated with anomalous winds in the upper troposphere/stratosphere at high latitudes which are communicated to the lower troposphere and are associated with surface MSLP anomalies. The surface winds act to change the mixing of heat up from the subsurface thermal maximum in the Labrador Sea and are thus related to a change in SSTs in this region. Evaporation in this region increases with SST and results in a salinification of the surface waters of the Labrador Sea. This salinity driven change in density in the Labrador Sea alters the background state and stability of the water column making it more likely that individual convective events, which are generally thermally driven, can occur and is shown by an increase in the mixed layer volume of the Labrador Sea. An increase in deep convection in the Labrador Sea thus leads a strengthening of the southward travelling deep western boundary current and a strengthening of the AMOC.

4.5 A note on the AMOC weakening

Following a maximum around 1920 the AMOC subsequently declines in NAT (Fig. 2, blue). Associated with the AMOC decline is a sharp reduction in Labrador Sea convection, depicted by the Labrador Sea mixed layer volume (Fig. 3a), followed by a decade of very little convection notable also for the lack of interannual variability (not shown). This is led by a reduction in density which is driven by the continued increase in temperature of the

water column in the North Atlantic (Fig. 4a). This represents a negative feedback of the AMOC. Although the initial warming was due to surface fluxes, the subsequent increase is due to the increased northwards transport of heat by the strengthened overturning circulation, the upper branch of which extends down to around 800 m.

During the period 1930–1970 the mechanism of AMOC weakening is the reverse of the 1880–1920 strengthening phase and is as described in the previous sections. However, one notable difference in the oceanic part of the mechanism which breaks some of the symmetry between the two periods is the relative role of temperature and salinity in the Labrador Sea density anomalies. Prior to the period beginning in 1930 the AMOC has already strengthened causing an increase in northward heat transport (not shown) which reduces the top 800 m column integrated density. Thus the declining density during the beginning of the 20th century in NAT is a combination of both the increased heat content of the Labrador Sea region and the declining evaporation. From 1930 to 1970 the surface buoyancy fluxes and associated atmospheric forcing are approximately the inverse of the 1880–1920 AMOC strengthening phase but are acting on a water column which is also partially becoming more stable due to the AMOC itself.

5 Climate impacts

We have shown that, in this model, despite the increase in volcanism in the 1880s, volcanic forcing alone was not the dominant natural forcing during this time in terms of the large scale ocean circulation response in the North Atlantic. However, direct application to 19th and 20th Century climates is complicated by the lack of anthropogenic forcings and uncertainty in the level of solar forcing prior to the satellite era (Forster et al. 2007). Nonetheless, with caveats associated with a study of one model, these results show that solar variability could help to force significant changes in the ocean circulation which may then be expected to have impacts on the wider climate; these impacts are now discussed.

To first order, in the context of natural forcings alone: large, globally-averaged surface air temperature (SAT) anomalies are volcanically rather than solar forced (they are seen in NAT as well as in NOSOL) in HadGEM2-ES, with a reduction in global SAT following increased volcanic activity (Fig. 11a), such as in the 1880s and in the late 20th Century. However, there are several decades in the early 20th Century where the global SAT in NAT and NOSOL show large and sustained contrasts. This is most likely due to the redistribution of heat associated with increased northward heat transport by the Atlantic ocean, which is very
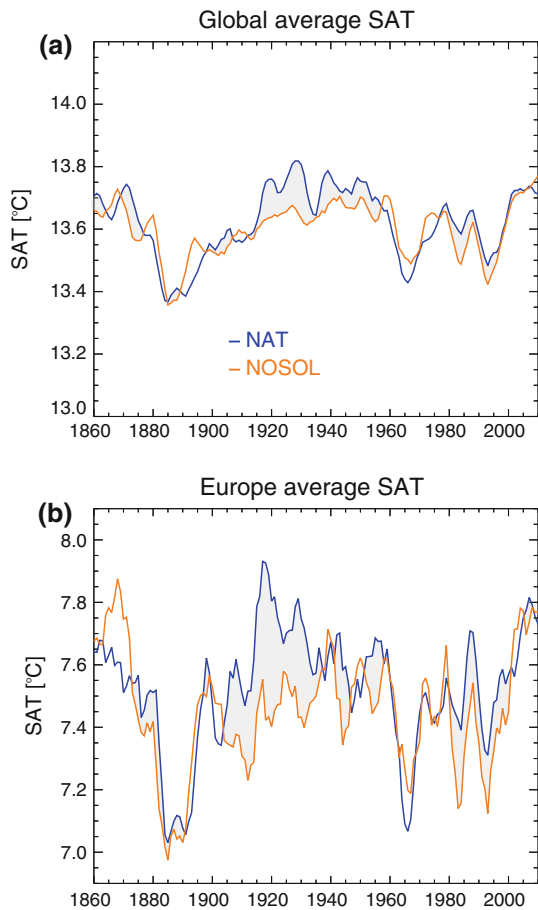
Fig. 11 Time series of (*top*) global and (*bottom*) annual mean European (10°W–90°E, 30°N–60°N) average temperature at 1.5 m (surface air temperature, SAT) in NAT (*blue*) and NOSOL (*orange*). *Grey shading* is applied where SAT in NAT is greater than in NOSOL. To allow for comparison of absolute magnitudes, y-axis tick spacings are equal in both panels

highly correlated with the AMOC (Menary et al. 2013). This results in anomalously high land temperatures downstream of the warmer North Atlantic, with the Eurasian continent warming by 0.3 °C in NAT compared to NOSOL for the 20 year period (from 1905 to 1925) in phase with the strengthening of the AMOC (Fig. 11b). Regression analysis using the control simulation suggests the NAO in NAT during this time can explain at most only 10 % of this signal directly, suggesting a crucial role for Atlantic heat transport. From the low annual Eurasian temperatures following the volcanism of the 1880s (e.g. Krakatoa 1883) there is an increase of almost 1 °C to the temperatures coinciding with the AMOC maximum in the 1920s. This is in contrast to NOSOL where Eurasian temperatures recover more slowly and to a lesser extent.

Within the larger group of CMIP5 experiments performed with HadGEM2-ES (Jones et al. 2011), the AMOC response in the NAT ensemble is different to the AMOC
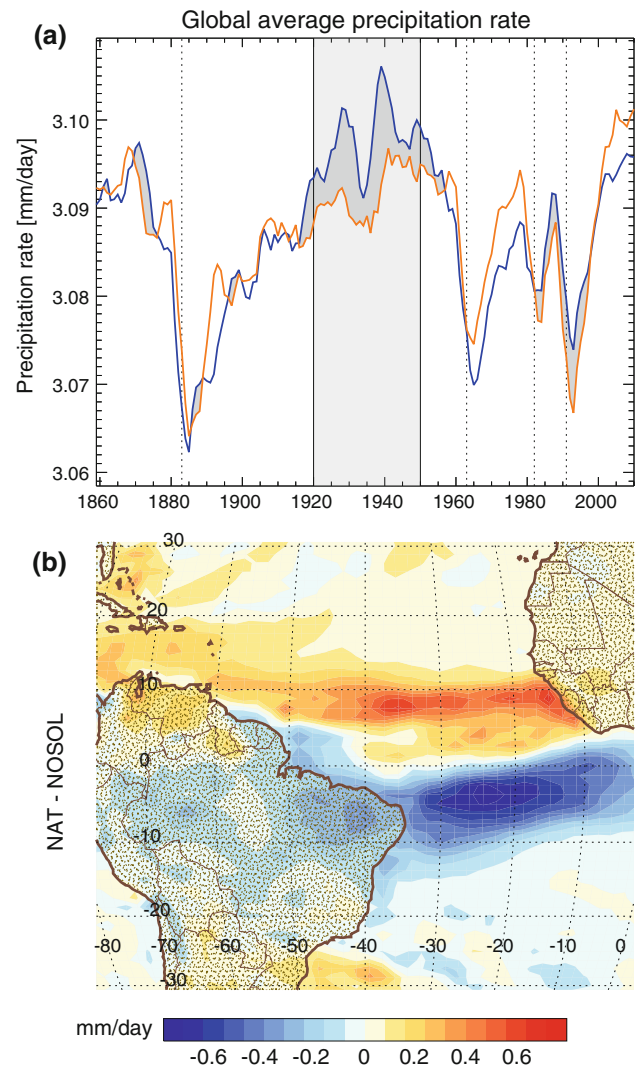
Fig. 12 *Top* global average precipitation rate in NAT (*blue*) and NOSOL (*orange*) with regions where precipitation rate in NAT is greater than in NOSOL shaded *dark grey*. *Dotted lines* denote major volcanic eruptions which from *left* to *right* are Krakatoa (1883), Agung (1963), El Chichón (1982), and Pinatubo (1991). *Bottom* difference between years 1920–1950 in NAT and years 1920–1950 in NOSOL, as indicated by *light grey shaded* region in *upper panel*

response simulated under the ALL-forcings scenario (including anthropogenic aerosols and GHGs, land-use changes, as well as the solar and volcanic forcing in NAT). In the ALL simulations, which are designed to be a best estimate of the actual historical forcing given the constraints of the model, the AMOC strengthens approximately linearly over a period of about 150 years due to the approximately linear increase in aerosol forcing in the northern hemisphere (Menary et al. 2013). In the ALL simulations there is also a multidecadally varying signature in North Atlantic SSTs (NASSTs; Booth et al. 2012) related to local shortwave forcing due to the multidecadal variability in aerosol emissions superposed on the linear

trend [see Figure 2c of Booth et al. (2012)]. The magnitude of the NASST variability due to anthropogenic aerosol forcing investigated by Booth et al. (2012) is larger than that due to solar forcing (i.e. NAT minus NOSOL) investigated here. However, when anthropogenic aerosols are removed in those experiments there is still some multidecadal variability in NASSTs [see Figure 2a of Booth et al. (2012)], which suggests there may be some role for solar forcing in the NASST response in HadGEM2-ES.

In the context of only natural forcings: large global precipitation anomalies are again primarily volcanically rather than solar forced, with a reduction in global precipitation following increased volcanic activity (Fig. 12a), similar to the SAT response. However, associated with the strengthening AMOC and northward heat transport in NAT (as compared to NOSOL), there is a northward shift of the ITCZ (Fig. 12b) related to the increased cross-equatorial SST gradient consistent with previous multi-model work including a precursor to this model (Menary et al. 2012; Vellinga and Wu 2004). This northward shift is associated with a sustained decrease in Amazonian rainfall of around 0.13 mm/day between 1920 and 1950 (difference between NAT and NOSOL), following the period of the anomalously strong AMOC.

Paleoclimate records show that around 1,000 years ago the climate of the northern hemisphere entered a multicentury long warm phase, known as the Medieval Warm Period (MWP), with northern hemisphere temperatures rising by around 0.3 °C (Jansen et al. 2007). Subsequently, between the MWP and Little Ice Age (LIA; 17th to 19th centuries) there was a gradual reduction in northern hemisphere surface temperatures by around 0.5°, though neither of these changes is spatially or temporally uniform and the magnitude is uncertain (Jansen et al. 2007). Given these temperature changes and the relationship between the modelled AMOC and European temperatures derived in this study, our model would predict a multidecadal timescale strengthening of the AMOC in reality by around 1.5 Sv followed by a hiatus and a subsequent gradual weakening of the AMOC by around 2 Sv. Though critically comparing these values with the observed record is difficult, the latter magnitude is broadly consistent with proxy evidence of changes in Florida Strait transport (Lund et al. 2006). It remains unclear though how, and indeed why, the AMOC would remain in its strengthened state rather than rebounding, and why the AMOC decline would be gradual rather than similarly paced to the strengthening. Other recent modelling work suggests that idealised solar forcing can excite various multidecadal to centennial timescale internal modes of variability within the AMOC (Park and Latif 2012). Using the model in the current study, further experiments over longer periods with solar variability imposed would be useful in this context.

Multidecadal (rather than multicentennial) timescale transitions, as demonstrated in this model study as a consequence of natural forcings, are consistent with some proxies of northern hemisphere SAT over the last millennium (D'Arrigo et al. 2006; Esper et al. 2002), whereas others suggest longer timescale changes (Moberg et al. 2005; Hegerl et al. 2006). Previous modelling studies with simpler models spanning the last millennium show a general cooling of northern hemisphere temperatures in agreement with the paleo proxies (Jansen et al. 2007), though of those models reviewed by Jansen et al. (2007) neither of the global non-flux adjusted coupled models extending back to the MWP reported results for the AMOC (Gonzalez-Rouco et al. 2003; Osborn et al. 2006). On shorter and more recent timescales, the Arctic warming of the early 20th Century (Wood and Overland 2010) also bears some similarities to the decadal timescale differences between NAT and NOSOL in SAT north of 60°N. The leading cause of this anomaly is thought to be the sustained positive NAO anomaly for approximately a decade from the beginning of the 20th Century which compares well to our simulated positive NAO-like anomaly during a similar time.

6 Conclusions

This study has investigated the ensemble mean oceanic response of a state-of-the-art climate model to solely natural forcings over the last 150 years. The AMOC is shown to exhibit large, sustained multidecadal variability in response to solar variability, strengthening by 1.5 Sv to a maximum of 14.5 Sv (11-year mean) over 50 years, before subsequently declining by 1.9 Sv to a minimum of 12.6 Sv (11-year mean) over a similar period of time. This follows a period of strong volcanism in the 1880s, most notably the Krakatoa eruption of August 1883. However, experiments with volcanic forcing only (NOSOL), entirely parallel to the NAT experiments, initialised from the same points in the long pre-industrial control run of the model, showed no significant changes in the strength of the AMOC, suggesting that volcanic forcing alone was not able to force this AMOC increase and that this increase is due to solar forcing or the non-linear combination of solar and volcanic forcing.

The proposed mechanism (Fig. 10) relates solar forcing to a change in the stratospheric circulation and MSLP which is reproducible in this model but somewhat different to some previous work (Ineson et al. 2011) perhaps due to the different timescale or perhaps due to the model's limited stratospheric resolution. Nevertheless, for this model, the results show the potential for small perturbations in solar forcing to affect atmospheric circulation through the depth of the stratosphere and troposphere.

Analysis of the mechanisms driving the AMOC increase show that it is driven by changes in deep water formation in the North Atlantic as a response to changes in the surface freshwater budget. Anomalous evaporation results in a destabilization of the water column in the Labrador Sea. The evaporation changes are due to persistent positive zonal wind anomalies. After the AMOC strengthening is a period of long term weakening which is associated with the increased advective heat fluxes due to the strengthened AMOC which oppose the surface salinity changes. Subsequently the AMOC weakens still further and overshoots its initial strength. This weakening overshoot is related to the opposite cycle of the proposed mechanism but also reflects some of the inertia of the large scale ocean system.

A sustained (i.e. multidecadal) change in the AMOC amounting to an increase of 1.5 Sv, followed by a decrease of 1.9 Sv, could have significant climate impacts due to the way in which the AMOC effectively amplifies external forcing. In NAT a northwards shift of the ITCZ as a result of the increased northwards heat transport associated with a stronger AMOC (Menary et al. 2012) results in a decrease in Amazonian rainfall of 0.13 mm/day for three decades, a relationship also seen in observations (Yoon and Zeng 2010). Similarly, recent droughts in Amazonia may also be related to Atlantic, rather than Pacific, SSTs (Marengo et al. 2008; Lewis et al. 2011).

Finally, an analysis of the effect of the AMOC strengthening on Eurasian land temperatures shows an anomalous warming of 0.5 °C for the 20 year period 1905–1925 during which the AMOC is strengthening. This Eurasian warming might be expected as the response to a strengthening AMOC (Sutton and Hodson 2005) but rather than being forced by internal variability it is shown here to be the response (via the AMOC) to natural climate forcings, of which of first order importance (in terms of the AMOC response) is solar forcing. Is it plausible that such an AMOC strengthening could be sustained, given the right external forcing? If so, this mechanism may be useful in contributing to explanations of the origins of the Medieval Warm Period and subsequent Little Ice Age northern hemisphere temperature anomalies as well as multidecadal climate variability in and around the Atlantic basin.

References

Bellouin N, Boucher O, Haywood J, Johnson C, Jones A, Rae J, Woodward S (2011) Improved representation of aerosols for HadGEM2. Hadley Centre Technical Note 73. Met Office Hadley Centre, Exeter, UK, 43 pp

Booth B, Dunstone N, Halloran P, Bellouin N, Andrews T (2012) Aerosols indicated as prime driver of 20th century North Atlantic climate variability. Nature 484(7393):228–232

Collins WJ, Bellouin N, Doutriaux-Boucher M, Gedney N, Halloran P, Hinton T, Hughes J, Jones CD, Joshi M, Liddicoat S, Martin G, O'Connor F, Rae J, Senior C, Sitch S, Totterdell I, Wiltshire A, Woodward S (2011) Development and evaluation of an earth-system model hadgem2. Geosci Model Dev 4(4):1051–1075. doi:10.5194/gmd-4-1051-2011

Cunningham SA, Kanzow T, Rayner D, Baringer MO, Johns WE, Marotzke J, Longworth HR, Grant EM, Hirschi JJM, Beal LM, Meinen CS, Bryden HL (2007) Temporal variability of the Atlantic meridional overturning circulation at 26.5 degrees N. Science 317(5840):935–938. doi:10.1126/science.1141304

D'Arrigo R, Wilson R, Jacoby G (2006) On the long-term context for late twentieth century warming. J Geophys Res-Atmos 111(D3) doi:10.1029/2005JD006352

Delworth T, Manabe S, Stouffer R (1993) Interdecadal variations of the thermohaline circulation in a coupled ocean-atmosphere model. J Clim 6(11):1993–2011. doi:10.1175/1520-0442(1993)006<1993:IVOTTC>2.0.CO;2

Dong B, Sutton R (2005) Mechanism of interdecadal thermohaline circulation variability in a coupled ocean-atmosphere GCM. J Clim 18(8):1117–1135

Dong B, Sutton R, Scaife A (2006) Multidecadal modulation of El Nino-Southern Oscillation (ENSO) variance by Atlantic Ocean sea surface temperatures. Geophys Res Lett 33(8) doi:10.1029/2006GL025766

Esper J, Cook E, Schweingruber F (2002) Low-frequency signals in long tree-ring chronologies for reconstructing past temperature variability. Science 295(5563):2250–2253. doi:10.1126/science.1066208

Forster P, Ramaswamy V, Artaxo P, Berntsen T, Betts R, Fahey D, Haywood J, Lean J, Lowe D, Myhre G, Nganga J, Prinn R, Raga G, Schutz M, Van Dorland R (2007) Changes in atmospheric constituents and in radiative forcing. In: Climate change 2007: the physical science basis contribution of working Group I to the fourth assessment report of the intergovernmental panel on climate change

Gonzalez-Rouco F, von Storch H, Zorita E (2003) Deep soil temperature as proxy for surface air-temperature in a coupled model simulation of the last thousand years. Geophys Res Lett 30(21) doi:10.1029/2003GL018264

Goosse H, Renssen H (2006) Regional response of the climate system to solar forcing: the role of the ocean. Space Sci Rev 125(1–4):227–235 doi:10.1007/s11214-006-9059-0, ISSI workshop on solar variability and planetary climates, Bern, Switzerland, 06–10 June 2005

Gordon C, Cooper C, Senior C, Banks H, Gregory J, Johns T, Mitchell J, Wood R (2000) The simulation of SST, sea ice extents and ocean heat transports in a version of the Hadley Centre coupled model without flux adjustments. Clim Dyn 16(2–3):147–168

Hawkins E, Smith RS, Allison LC, Gregory JM, Woollings TJ, Pohlmann H, de Cuevas B (2011) Bistability of the Atlantic overturning circulation in a global climate model and links to ocean freshwater transport. Geophys Res Lett 38. doi:10.1029/2011GL047208

Hegerl G, Crowley T, Hyde W, Frame D (2006) Climate sensitivity constrained by temperature reconstructions over the past seven centuries. Nature 440(7087):1029–1032. doi:10.1038/nature04679

Ineson S, Scaife AA, Knight JR, Manners JC, Dunstone NJ, Gray LJ, Haigh JD (2011) Solar forcing of winter climate variability in the Northern Hemisphere. Nat Geosci 4(11):753–757. doi:10.1038/NGEO1282

Iwi A, Hermanson L, Haines K, Sutton R (2012) Mechanisms linking volcanic aerosols to the Atlantic meridional overturning circulation. J Clim. doi:10.1175/2011JCLI4067.1

Jansen E, Overpeck J, Briffa K, Duplessy J, Joos F, Masson-Delmotte V, Olago D, Otto-Bliesner B, Peltier W, Rahmstorf S, Ramesh R, Raynaud D, Rind D, Solomina O, Villalba R, Zhang D (2007) Palaeoclimate. In: Climate change 2007: the physical science basis contribution of working Group I to the fourth assessment report of the intergovernmental panel on climate change

Jayne S, Marotzke J (2001) The dynamics of ocean heat transport variability. Rev Geophys 39(3):385–411. doi:10.1029/2000RG000084

Johns T, Durman C, Banks H, Roberts M, McLaren A, Ridley J, Senior C, Williams K, Jones A, Rickard G, Cusack S, Ingram W, Crucifix M, Sexton D, Joshi M, Dong B, Spencer H, Hill R, Gregory J, Keen A, Pardaens A, Lowe J, Bodas-Salcedo A, Stark S, Searl Y (2006) The new Hadley Centre climate model (HadGEM1): evaluation of coupled simulations. J Clim 19(7):1327–1353. doi:10.1175/JCLI3712.1

Jones CD, Hughes JK, Bellouin N, Hardiman SC, Jones GS, Knight J, Liddicoat S, O'Connor FM, Andres RJ, Bell C, Boo KO, Bozzo A, Butchart N, Cadule P, Corbin KD, Doutriaux-Boucher M, Friedlingstein P, Gornall J, Gray L, Halloran PR, Hurtt G, Ingram WJ, Lamarque JF, Law RM, Meinshausen M, Osprey S, Palin EJ, Chini LP, Raddatz T, Sanderson MG, Sellar AA, Schurer A, Valdes P, Wood N, Woodward S, Yoshioka M, Zerroukat M (2011) The HadGEM2-ES implementation of CMIP5 centennial simulations. Geoscientific Model Development 4(3):543–570. doi:10.5194/gmd-4-543-2011

Kanzow T, Cunningham SA, Johns WE, Hirschi JJM, Marotzke J, Baringer MO, Meinen CS, Chidichimo MP, Atkinson C, Beal LM, Bryden HL, Collins J (2010) Seasonal variability of the Atlantic meridional overturning circulation at 26.5 degrees N. J Clim 23(21):5678–5698. doi:10.1175/2010JCLI3389.1

Kara A, Rochford P, Hurlburt H (2000) An optimal definition for ocean mixed layer depth. J Geophys Res-Oceans 105(C7):16,803–816, 821. doi:10.1029/2000JC900072

Knight J, Allan R, Folland C, Vellinga M, Mann M (2005) A signature of persistent natural thermohaline circulation cycles in observed climate. Geophys Res Lett 32(20) doi:10.1029/2005GL024233

Kodera K, Kuroda Y (2002) Dynamical response to the solar cycle. J Geophys Res: Atmos 107(D24):ACL5–1–ACL5–12. doi:10.1029/2002JD002224

Kuhlbrodt T, Griesel A, Montoya M, Levermann A, Hofmann M, Rahmstorf S (2007) On the driving processes of the Atlantic meridional overturning circulation. Rev Geophys 45(1) doi:10.1029/2004RG000166

Levermann A, Griesel A, Hofmann M, Montoya M, Rahmstorf S (2005) Dynamic sea level changes following changes in the thermohaline circulation. Clim Dyn 24(4):347–354. doi:10.1007/s00382-004-0505-y

Lewis SL, Brando PM, Phillips OL, van der Heijden GMF, Nepstad D (2011) The 2010 Amazon drought. Science 331(6017):554. doi:10.1126/science.1200807

Lund DC, Lynch-Stieglitz J, Curry WB (2006) Gulf Stream density structure and transport during the past millennium. Nature 444(7119):601–604. doi:10.1038/nature05277

Manzini E, Cagnazzo C, Fogli PG, Bellucci A, Mller WA (2012) Stratosphere-troposphere coupling at inter-decadal time scales: implications for the north atlantic ocean. Geophys Res Lett 39(5). doi:10.1029/2011GL050771

Marengo JA, Nobre CA, Tomasella J, Oyama MD, De Oliveira GS, De Oliveira R, Camargo H, Alves LM, Brown IF (2008) The drought of Amazonia in 2005. J Clim 21(3):495–516. doi:10.1175/2007JCLI1600.1

Martin GM, Bellouin N, Collins WJ, Culverwell ID, Halloran PR, Hardiman SC, Hinton TJ, Jones CD, McDonald RE, McLaren AJ, O'Connor FM, Roberts MJ, Rodriguez JM, Woodward S, Best MJ, Brooks ME, Brown AR, Butchart N, Dearden C, Derbyshire SH, Dharssi I, Doutriaux-Boucher M, Edwards JM, Falloon PD, Gedney N, Gray LJ, Hewitt HT, Hobson D, Huddleston MR, Hughes J, Ineson S, Ingram WJ, James PM, Johns TC, Johnson CE, Jones A, Jones CP, Joshi MM, Keen AB, Liddicoat S, Lock AP, Maidens AV, Manners JC, Milton SF, Rae JGL, Ridley JK, Sellar A, Senior CA, Totterdell IJ, Verhoef A, Vidale PL, Wiltshire A, Team HD (2011) The HadGEM2 family of Met Office Unified Model climate configurations. Geosci Model Dev 4(3):723–757. doi:10.5194/gmd-4-723-2011

McManus J, Francois R, Gherardi J, Keigwin L, Brown-Leger S (2004) Collapse and rapid resumption of Atlantic meridional circulation linked to deglacial climate changes. Nature 428(6985):834–837. doi:10.1038/nature02494

Meehl G, Stocker T, Collins W, Friedlingstein P, Gaye A, Gregory J, Kitoh A, Knutti R, Murphy J, Noda A, Raper S, Watterson I, Weaver A, Zhao Z (2007) Chapter 10: global climate projections. In: Climate change 2007: the physical science basis contribution of working Group I to the fourth assessment report of the intergovernmental panel on climate change

Menary MB, Roberts CD, Palmer MD, Halloran PR, Jackson L, Wood RA, Muller WA, Matei D, Lee SK (2013) Mechanisms of aerosol-forced amoc variability in a state of the art climate model. J Geophys Res: Oceans 118(4):2087–2096. doi:10.1002/jgrc.20178

Menary MB, Park W, Lohmann K, Vellinga M, Palmer MD, Latif M, Jungclaus JH (2012) A multimodel comparison of centennial Atlantic meridional overturning circulation variability. Clim Dyn 38(11–12):2377–2388. doi:10.1007/s00382-011-1172-4

Mignot J, Ganopolski A, Levermann A (2007) Atlantic subsurface temperatures: response to a shutdown of the overturning circulation and consequences for its recovery. J Clim 20(19):4884–4898. doi:10.1175/JCLI4280.1

Mignot J, Khodri M, Frankignoul C, Servonnat J (2011) Volcanic impact on the Atlantic Ocean over the last millennium. Clim Past 7(4):1439–1455. doi:10.5194/cp-7-1439-2011

Moberg A, Sonechkin D, Holmgren K, Datsenko N, Karlen W (2005) Highly variable Northern Hemisphere temperatures reconstructed from low- and high-resolution proxy data. Nature 433(7026):613–617. doi:10.1038/nature03265

Moreno A, Stoll H, Jimenez-Sanchez M, Cacho I, Valero-Garces B, Ito E, Edwards RL (2010) A speleothem record of glacial (25-11.6 kyr BP) rapid climatic changes from northern Iberian Peninsula. Global And Planetary Change 71(3–4, Sp. Iss. SI) pp 218–231 doi:10.1016/j.gloplacha.2009.10.002

Morgenstern O, Braesicke P, O'Connor FM, Bushell AC, Johnson CE, Osprey SM, Pyle JA (2009) Evaluation of the new ukca climate-composition model part 1: the stratosphere. Geosci Model Dev 2(1):43–57. doi:10.5194/gmd-2-43-2009

Osborn TJ, Raper SCB, Briffa KR (2006) Simulated climate change during the last 1,000 years: comparing the ECHO-G general circulation model with the MAGICC simple climate model. Clim Dyn 27(2–3):185–197. doi:10.1007/s00382-006-0129-5

Park W, Latif M (2012) Atlantic meridional overturning circulation response to idealized external forcing. Clim Dyn 39:1709–1726. doi:10.1007/s00382-011-1212-0

Pohlmann H, Sienz F, Latif M (2006) Influence of the multidecadal Atlantic meridional overturning circulation variability on European climate. J Clim 19(23):6062–6067. doi:10.1175/JCLI3941.1

Rahmstorf S (2003) The current climate. Nature 421(6924):699. doi:10.1038/421699a

Reichler T, Junsu K, Manzini E, Kroger J (2012) A stratospheric connection to Atlantic climate variability. Nature Geosci 5(11):783–787. doi:10.1038/ngeo1586

Roberts CD, Palmer MD (2012) Detectability of changes to the atlantic meridional overturning circulation in the hadley centre climate models. Clim Dyn 39(9–10):2533–2546

Roberts CD, Garry FK, Jackson LC (2013) A multimodel study of sea surface temperature and subsurface density fingerprints of the atlantic meridional overturning circulation. J Clim 26(22):9155–9174

Sato M, Hansen J, McCormick M, Pollack J (1993) Stratospheric aerosol optical depths, 1850–1990. J Geophys Res-Atmos 98(D12):22987–22994. doi:10.1029/93JD02553

Sedlacek J, Mysak LA (2009) A model study of the Little Ice Age and beyond: changes in ocean heat content, hydrography and circulation since 1500. Clim Dyn 33(4):461–475. doi:10.1007/s00382-008-0503-6

Semenov VA, Latif M, Dommenget D, Keenlyside NS, Strehz A, Martin T, Park W (2010) The Impact of North Atlantic-Arctic multidecadal variability on northern hemisphere surface air temperature. J Clim 23(21):5668–5677. doi:10.1175/2010JCLI3347.1

Stenchikov G, Delworth TL, Ramaswamy V, Stouffer RJ, Wittenberg A, Zeng F (2009) Volcanic signals in oceans. J Geophys Res-Atmos, vol 114. doi:10.1029/2008JD011673

Stott PA, Jones GS, Lowe JA, Thorne P, Durman C, Johns TC, Thelen JC (2006) Transient climate simulations with the HadGEM1 climate model: causes of past warming and future climate change. J Clim 19(12):2763–2782. doi:10.1175/JCLI3731.1

Sutton R, Hodson D (2005) Atlantic Ocean forcing of North American and European summer climate. Science 309(5731):115–118. doi:10.1126/science.1109496

Swingedouw D, Terray L, Cassou C, Voldoire A, Salas-Melia D, Servonnat J (2011) Natural forcing of climate during the last millennium: fingerprint of solar variability. Clim Dyn 36(7–8):1349–1364. doi:10.1007/s00382-010-0803-5

Timmermann A, Okumura Y, An SI, Clement A, Dong B, Guilyardi E, Hu A, Jungclaus JH, Renold M, Stocker TF, Stouffer RJ, Sutton R, Xie SP, Yin J (2007) The influence of a weakening of the Atlantic meridional overturning circulation on ENSO. J Clim 20(19):4899–4919. doi:10.1175/JCLI4283.1

Vellinga M, Wood RA (2008) Impacts of thermohaline circulation shutdown in the twenty-first century. Clim Change 91(1–2):43–63. doi:10.1007/s10584-006-9146-y

Vellinga M, Wu P (2004) Low-latitude freshwater influence on centennial variability of the Atlantic thermohaline circulation. J Clim 17(23):4498–4511

Wood KR, Overland JE (2010) Early 20th century Arctic warming in retrospect. Int J Climatol 30(9):1269–1279. doi:10.1002/joc.1973

Wood R, Vellinga M, Thorpe R (2003) Global warming and thermohaline circulation stability. Philos Trans R Soc Lond Ser A-Math Phys Eng Sci 361(1810):1961–1974. doi:10.1098/rsta.2003.1245

Yoon JH, Zeng N (2010) An Atlantic influence on Amazon rainfall. Clim Dyn 34(2–3):249–264. doi:10.1007/s00382-009-0551-6

Zanchettin D, Timmreck C, Graf HF, Rubino A, Lorenz S, Lohmann K, Krger K, Jungclaus J (2011) Bi-decadal variability excited in the coupled oceanatmosphere system by strong tropical volcanic eruptions. Clim Dyn, pp 1–26. doi:10.1007/s00382-011-1167-1

Zhang R, Delworth TL (2006) Impact of Atlantic multidecadal oscillations on India/Sahel rainfall and Atlantic hurricanes. Geophys Res Lett 33(17) doi:10.1029/2006GL026267

Zhang R, Vallis GK (2007) The role of bottom vortex stretching on the path of the north Atlantic western boundary current and on the northern recirculation gyre. J Phys Oceanogr 37(8):2053–2080. doi:10.1175/JPO3102.1

Zhong Y, Miller GH, Otto-Bliesner BL, Holland MM, Bailey DA, Schneider DP, Geirsdottir A (2011) Centennial-scale climate change from decadally-paced explosive volcanism: a coupled sea ice-ocean mechanism. Clim Dyn 37(11–12):2373–2387. doi:10.1007/s00382-010-0967-z

Zorita E, Von Storch H, Gonzalez-Rouco F, Cubasch U, Luterbacher J, Legutke S, Fischer-Bruns I, Schlese U (2004) Climate evolution in the last five centuries simulated by an atmosphere-ocean model: global temperatures, the North Atlantic Oscillation and the Late Maunder Minimum. Meteorol Z 13(4):271–289. doi:10.1127/0941-2984/2004/0013-0271